Optik - International Journal for Light and Electron Optics 274 (2023) 170565

Contents lists available at ScienceDirect

Optik

journal homepage: www.elsevier.com/locate/ijleo

First-principles calculations to investigate structural, elastic, electronic, optical, and magnetic properties of Hg_2WO_4 for photocatalytic applications

Sania Ayub [a], Adnan Khalil [a,*], Rahila Shaheen [a], Soumaya Gouadria [b], Muhammad Bilal Tahir [a,c], Zaka Ullah [d], Abdul Hannan [a], El Sayed Yousef [e,f], Meshal Alzaid [g]

[a] Institute of Physics, Khwaja Fareed University of Engineering and Information Technology, Rahim Yar Khan 64200, Pakistan
[b] Department of Physics, College of Science, Princess Nourah bint Abdulrahman University, P.O. Box 84428, Riyadh 11671, Saudi Arabia
[c] Centre for Innovative Material Research, Khwaja Fareed University of Engineering and Information Technology, Rahim Yar Khan 64200, Pakistan
[d] Department of Physics, Division of Science and Technology, University of Education, Lahore 54770, Pakistan
[e] Research Center for Advanced Materials Science (RCAMS), King Khalid University, P.O. Box 9004, Abha 61413, Saudi Arabia
[f] Physics Department, Faculty of Science, King Khalid University, P. O. Box 9004, Abha, Saudi Arabia
[g] Department of Physics, College of Science, Jouf University, Al-Jouf, Sakaka, P.O. Box 2014, Saudi Arabia

ARTICLE INFO

Keywords:
Photosensitive
DFT
Antiferromagnetic
Optical
Photocatalytic

ABSTRACT

In the present work, structural, elastic, electronic, optical, and magnetic properties of Hg_2WO_4 are investigated using CASTEP simulation tool. Generalized Gradient Approximation (GGA) along with Perdew-Burke-Ernzerhof (PBE) are employed for the calculation of electronic exchange and correlation energy. In structural analysis, Hg_2WO_4 is found to be stable with C-centered monoclinic structure having space group C2/c. Material's ductile nature is confirmed with Pugh's approximation where calculated B/G ratio is greater than 0.75 and Frantsevich's rule where v is greater than 0.26. The calculations of electronic properties show that Hg_2WO_4 has indirect band gap of 2.14 eV. While the optical study reveals that Hg_2WO_4 has a good photosensitivity in visible light region. Furthermore, the spin-polarized treatment shows that Hg_2WO_4 is antiferromagnetic in nature. The current findings can be of great importance for the development of efficient photocatalytic materials for water splitting and associated applications.

1. Introduction

To address the energy crisis concerns, photocatalysis process is considered to be an effective approach for storing and conversion of solar energy [1]. The widely used metal oxide semiconductors provide efficient photocatalytic platform for water splitting in order to attain renewable hydrogen for cheap and clean power production. Owing to suitable composition and structural flexibility, layered perovskite materials with general formula A_2BX_4, have attracted extensive attentions for solar water splitting [2]. In this type of perovskite-like structure, the ABX_3 and AX patterns are repeated throughout the crystal [3]. This type of structural repetition makes it a class of Ruddlesden-Popper phase materials. A Ruddlesden-Popper phase is a layered perovskite structure in two-dimensional space

* Corresponding author.
E-mail address: Khalil.adnan2021@gmail.com (A. Khalil).

https://doi.org/10.1016/j.ijleo.2023.170565
Received 15 October 2022; Received in revised form 24 December 2022; Accepted 11 January 2023
Available online 13 January 2023

which follows the general formula $A_{n+1}B_nX_{3n+1}$. Alternatively, the formula for Ruddlesden-Popper phase can also be written as AO $(ABO_3)_n$ [4]. Generally, A and B sites are occupied by cations and X site is usually inhabited with anion species. A-site cations are located on the boundary which is sandwiched between two layers. The coordination number for A-site cations is 9. Whereas B-site cations are located at the center of octahedron that comprises six X-site anions [5].

These layered perovskite structures exhibit various physical properties including superconductivity [6], photoluminescence [7] and photocatalytic activity which are desired in versatile energy storage applications[8], [9]. The photocatalytic activity of widely studied TiO_2 is limited to UV-region only owing to its wide forbidden energy gap (3.2 eV). Since, the solar energy reaching to the surface of earth is approximately 36,000 TW per year [10] from which only 4% energy is carried by UV-light and its major portion fall in visible region (approximately 50%). This limitation has opened a door to develop visible-light-driven photocatalysts to meet the current and future requirements [11]. In addition to TiO_2, several other metal oxide semiconductors (MOSCs) are studied including WO_3, No and ZrO_2. Tungsten oxide (WO_3) based photocatalysts have band gap ranging from 2.6 to 2.8 eV which is useful for the fabrication of visible-light-driven semiconductor photocatalysts. This makes the material second most studied MOSCs after TiO_2 [12]. The valence band potential of WO_3 lies between 2.7 and 3.44 eV and its photocatalytic response is comparable to traditional TiO_2 photocatalyst. The notable photocatalytic performance is typically attributed to oxidation ability of generated hole-pairs in valence band of WO_3 which strongly depends on crystal orientations and structural defects [13]. Besides this, WO_3 is non-toxic and abundant in nature. In comparison to TiO_2, it is more suitable for photocatalytic water splitting [12], [14].

The photocatalytic activity of WO_3 is enhanced when it is fabricated in layered-perovskite structure which general formula A_2WO_4, where A is any transition or alkali metal. In this system, layers of AWO_3 and AO are repeated periodically assigning this system in the category of Ruddlesden-Popper phase. The proposed compound Hg_2WO_4 is thus gave suitable applications including superconductivity, water splitting, and photoluminescence. In literature, low-temperature modification of Hg_2WO_4 has been achieved using the hydrothermal recrystallization approach, for temperature as low as 180 °C. The structural properties of experimentally prepared Hg_2WO_4 were determined using the Guinier powder data method. The Hg_2WO_4 assembles in pale yellow color. The lattice constant *a* measured as 873.0 pm, *b* as 1147.6 pm and c as 493.05 pm [15]. Whereas the volume V is found as 0.4484 nm^3, space-group as C2/c, β as 115.196°, and z as 4 [16]. In this present work, we have focused on exploring the features of Hg_2WO_4 layered-perovskite compound through first-principles calculations [17], [18], [19], [20], [21] based on density functional theory [22], [23], [24] for photocatalytic activity involving water splitting. This computational work is implemented in CASTEP in order to investigate structural, electronic band structure, optical and, magnetic properties of Hg_2WO_4 [25], [26], [27]. As long as structural arrangements of layer perovskite oxide compounds are concerned, the perovskite-like materials are divided into two categories on the basis of their structural growth: T-type structure and T′-type structure. The T-type structure is usually possessed by ternary oxides A_2BO_4 which are composed of periodic repeated layers of ABO_3 and AO rock salt. Whereas, T′-type structure is composed of infinite layers of BO_2 along with intergrowth of A_2O_2 layers placed along the c-axis and inhibited with AO_8 cubes and BO_4 square planes that are corner-shared [28]. The structural stability of T and T′ type is investigated by implying schematic of Goldschmidt tolerance factor "t". The formula of "t" derived from the perovskite sub-cell, is given as:

$$t = \frac{(r_A + r_O)}{\sqrt{2}(r_B + r_O)}$$

Where r_{an} is the radius of A-ion, r_{ob} is the radius of B-ion, and r_{ob} is the radius of O-ion [29], [30]. It is found in literature that the tolerance factor *t* for phases which are consist with T-type structure, has the value as $0.87 < t < 0.99$, and for those T′ type, its value falls in the range of $0.83 < t < 0.86$ [31]. The A_2BO_4 oxide structure is stable if it has *t* within the range of $0.85 < t < 1.02$ [32]. Whereas, the tolerance factor 1 represents the ideal structure.

Here we employ the density functional theory (DFT) [33], [34], [35], [36] based on ab initio approach and use functional GGA-PBE for the investigation of structural, electronic and optical properties of perovskite-like material Hg_2WO_4. There are other approximation methods too such as Peso, HSE06 etc. where Peso is good for treating alkali metals or alkali halides while as long as cohesive energy concerned, PBE gives better calculations than Peso. Since no CASTEP simulations are done on investigating physical properties of Hg_2WO_4 so we have employed basic GGA-PBE approximations. We found that Hg_2WO_4 exhibit indirect band gap of 2.14 eV. The total density of states (TDOS) and the partial density of states (PDOS) are calculated for the investigation of electronic properties including band gap and position of Fermi level in Hg_2WO_4. Moreover, functions like absorption, reflectivity, refractive index, dielectric function, loss function, transmittance, resistivity and conductivity of Hg_2WO_4 are studied. The optical properties showed that Hg_2WO_4 has good photosensitivity for visible light. Furthermore, the magnetic behavior of the material is determined through application of magnetic field with spin-polarized treatment and we found that this compound is of antiferromagnetic nature. The study presents worthy outcomes for the development of Hg_2WO_4 based efficient photocatalysts for water splitting applications.

2. Computational methodology

Cambridge serial total energy package (CASTEP) simulation is based on DFT [37], [38], [39], [40]. Owing to its numerous capabilities, CASTEP is aimed to determine the physical properties of materials including liquids, surfaces, amorphous materials and crystalline structures. It utilizes first principle approach to calculate the basic quantity that is total energy. All other quantities are then derived from the basic quantity [41]. Functional like GGA and PBE are used for the calculation of electronic exchange and correlation energy [42] as it has been evidenced that when GGA functional is combined with local-density approximation (LDA), more accurate results are achieved [43]. In this manuscript, all calculations are executed on solving Kohn-Sham equations in the domain of density

functional theory [44], [45], [46], [47], [48]. Mercury (Hg), Tungsten (W), and Oxygen (O) pseudo-potentials with electronic configurations of 4 $f^{14}5d^{10}6\ s^2$, 6 $s^24\ f^1\ ^45d^4$, and 2 s^22p^4 respectively, are employed. Hg_2WO_4 shows the C-centered monoclinic crystal structure with space group C2/c. The cutoff energy is kept at 489.8 eV for performing convergence test. Using k-point mesh of $3 \times 3 \times 4$ for Hg_2WO_4 through Monkhorst-pack simulation, Brillouin zone has been sampled. The maximum displacement and maximum stress are found 0.0019 Å, and 0.1 GA respectively throughout the geometrical optimization [49]. The residual forces were kept controlled over the range of 0.04 eV/Å during structural relaxation [50].

3. Results and discussion

3.1. Structural and elastic properties

The structural properties of any material can be determined by finding its space group, atomic positions and lattice parameters. The Hg_2WO_4 has C-centered monoclinic crystal structure with space group C2/c [15]. The unit cell of Hg_2WO_4 is made up of four Hg atoms, two W atoms and eight O atoms. The conventional unit cell and primitive cell are shown in Fig. 1. The atomic position (also called Wyckoff positions) shows the location of atoms in a unit cell. In unit cell of Hg_2WO_4, Hg has positions 0.24, 0.47 and 0.96, W has positions 0.09, 0.9 and 0.25 whereas O has positions 0.04, 0.6 and 0.2. The lattice parameters determine the geometry of unit cell of a compound. The values of lattice parameters are found as a = b = 7.52 A°, c= 5.04 A°. Whereas, the volume, density and energy band gap of Hg_2WO_4 are respectively determined as 245.42 $Å^3$, 8.78 g cm^{-3} and 2.14 eV. Experimental structure of Hg_2WO_4 is also observed in [16] where values of lattice constants are a = 8.73 A°, b = 11.6 A°, c = 4.93 A°, and β = 114.86°. Comparison of experimental values and computationally calculated values shows that our calculated values are somehow consistent with experimentally calculated values and thus considered for further calculations. The geometrical optimization of Hg_2WO_4 is achieved at zero temperature and pressure, and the ground state properties are examined. GGA and PBE are used for the geometrical optimization. On applying Hill approximation, mechanical parameters like, shear modulus (G), bulk modulus (B), Young's modulus (Y), Pugh's ratio (B/G), Poisson's ratio (ν)and Pugh's modulus (G/B) for Hg_2WO_4 are investigated. The computed mechanical parameters and moduli of elasticity are listed in Table 1.

The medium range value of Bulk modulud (B) and Young;s modulud (Y) showed that Hg_2WO_4 is neither hard nor stiffer [51]. According to Pugh's approximation, if B/G > 1.75 the material is said to be ductile and for B/G < 1.75 the material showed brittle behavior. From Table 1, B/G ratio is 2.02 which is greater than 1.75 determine ductile nature of Hg_2WO_4. Ductile nature is also confirmed by Frantsevich's rule [52] which showed ductile nature for v > 0.26 and brittle for v < 0.26.

3.2. Electronic properties

DOS, PDOS and band structure of Hg_2WO_4 are calculated through energy exchange correlation function GGA/PBE and OTFG ultra soft pseudo potential method. Fig. 2 shows the electronic band structure of Hg_2WO_4 calculated along the symmetry points (also called k-points) of directions (L-M-A-G-Z-V) verses wave vectors of energy between − 5e V to 10 eV. The band structure describes the quantum mechanical behavior of electrons. It shows the allowed energy states of electrons in the solids. The highest energy level that can be occupied by an electron at zero absolute temperature is called Fermi level (E_F) and it has been denoted by dash line inside the band structure. The minimum of conduction band lies at a symmetry point while Z symmetry point is possessed the maxima of valence band, as shown in Fig. 2. The band gap is indirect and is calculated as 2.14 eV. The DFT always gives underestimated value of band gap, however, the density and atom type information are considered more accurate [19]. For water splitting, band gap value should be greater than 1.23 eV and less than 3 eV. Due to narrow band gap shown by Hg_2WO_4, it could be a potential candidate for

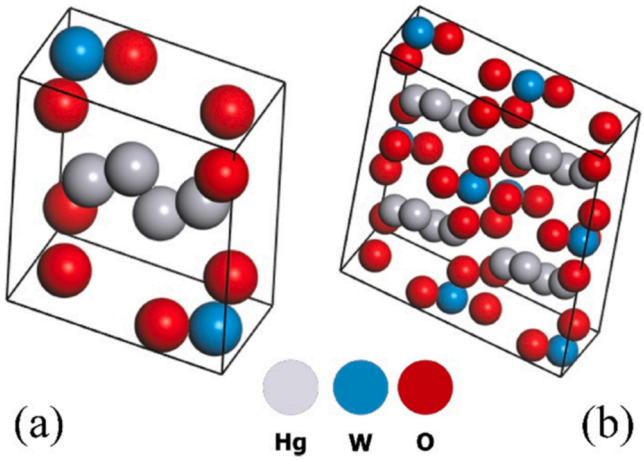

Fig. 1. Three-dimensional views showing the crystal structure of (a) primitive unit cell and (b) conventional unit cell of Hg_2WO_4.

Table 1
The mechanical parameters such as Bulk modulus "B" (GA), Shear modulus "G" (GA), Pugh's ratio "B/G," Young's modulus "Y" (GA), Pugh's modulus (G/B) and Poisson's coefficient "ν" for Hg_2WO_4 layered-oxide perovskite.

Compound	B	G	Y	ν	B/G	G/B
Hg_2WO_4	47.41725	23.41093	60.30772	0.28802	2.02	0.5

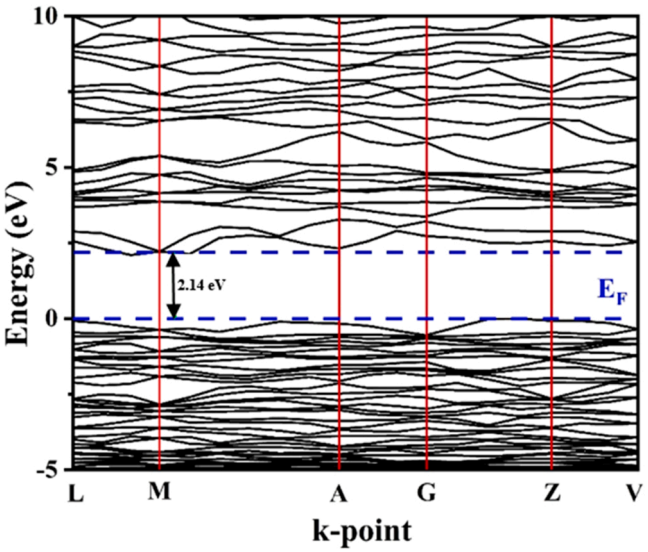

Fig. 2. Band structure of Hg_2WO_4.

photocatalytic applications such as water splitting.

The electronic features of Hg_2WO_4 are further studied by considering the PDOS and TDOS. Fig. 3(a) shows the TDOS for Hg_2WO_4. All the elemental and Hg_2WO_4 results have identical spectra and the peaks of all graphs meet at 28.86 states/eV and the DOS graph meets the Fermi level with 2.54 states/eV.

Fig. 3(b-d) shows the PDOS for Hg, O and Hg_2WO_4. In Hg, 5p and 5d orbitals contribute significantly and the main peak of Hg-6 s represents 2.4 states/eV. The main peak of Hg-5p possesses 14.03 states/eV while that of Hg-5d has the highest states as 22.7 states/eV. In case of O, the dominant contribution is from 2p state. The main peak of O-2p offers 13.47 states/eV and the O-2p curve meets the Fermi level at 1.34 states/eV. The results did not show any notable contribution of W. Fig. 3(c) shows that the O-2p and Hg-5d have dominant contribution in Hg_2WO_4. The main peak of D-DOS is recorded at 22.7 states/eV while that of p-DOS at 14.03 states/eV. Figure also shows the smaller contribution from s-DOS with peak at 2.4 states/eV, where the contribution of f-DOS is negligible. Moreover, s-DOS meets with the Fermi level at 1.02 states/eV and that of D-DOS at 0.1 states/eV.

3.3. Optical properties

Optical parameters determine the optical behavior of materials quantitatively. These parameters include coefficient of absorption, function of energy loss, dielectric constant, reflectivity, and index of refraction. These parameters are introduced in calculations when light (electromagnetic waves) interacts with matter. The optical properties are mutually linked with each another and one can help to determine the other. The complex dielectric function, function of frequency, have real and imaginary parts for the quantitative analysis of light interaction with matter. The Maxwell expression for complex dielectric function is given in Eq. 1:

$$\varepsilon(\omega) = \varepsilon_1(\omega) + i\varepsilon_2(\omega) \tag{1}$$

The real part of dielectric function ε_1 determines material's ability of interacting with incident light without absorbing it while imaginary part ε_2 represents transition between occupied and unoccupied electronic states while measuring material's ability to absorb light. Polarization of light within a material is determined with the help of real part of complex dielectric function which is represented as $\mathcal{E}_1$ (ω). Whereas the loss function, also known as energy dissipation, is estimated from imaginary part of dielectric function and is denoted by $\mathcal{E}_2$(ω) [49].

3.4. Reflectivity

Reflectivity can be determined from complex refractive index n($\mathcal{E}$). Whereas n(ω) has two parts: refractive index and extinction

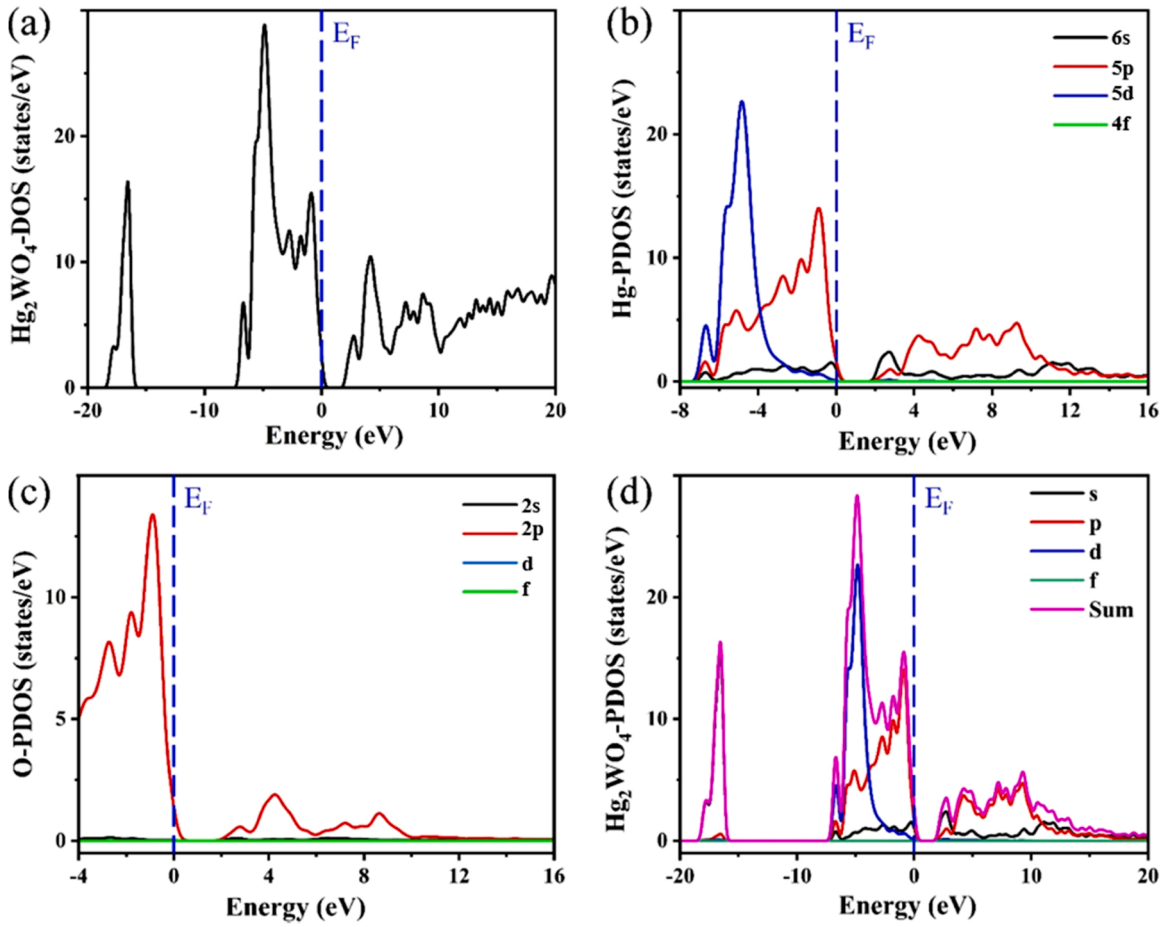

Fig. 3. TDOS of (a) Hg_2WO_4. PDOS of (b) Hg, (c) O and (d) Hg_2WO_4.

coefficient. Reflectivity is related to refractive index and extinction coefficient as follow:

$$R = \frac{(n-1)^2 + k^2}{(n+1)^2 + k^2} \tag{2}$$

The reflectivity response of Hg_2WO_4 is shown in Fig. 4(a). A peak value of reflectivity is found as 0.43 at 37.9 eV. Whereas, another notable peak is observed at 8.9 eV.

3.5. Absorption

The absorption coefficient is calculated from frequency of electromagnetic waves and complex dielectric function using the following relation:

$$A(\omega) = \frac{4\pi k(\omega)}{\lambda} \tag{3}$$

In equation 3, A(ω) represents the absorption coefficient. The absorption spectrum for Hg_2WO_4 is shown in Fig. 4(c). The threshold point of absorption which is the point at which maximum energy of incident light is absorbed by the material, is found as 6.1×10^5 at 32.7 eV. Transmittance can be calculated using given relation

$$T = 1 - \alpha(\omega) - R(\omega), \tag{4}$$

From Fig. 2, band gap of proposed material lies in visible range where material gives maximum absorption so transmittance is low in visible range while material is transparent in infrared region.

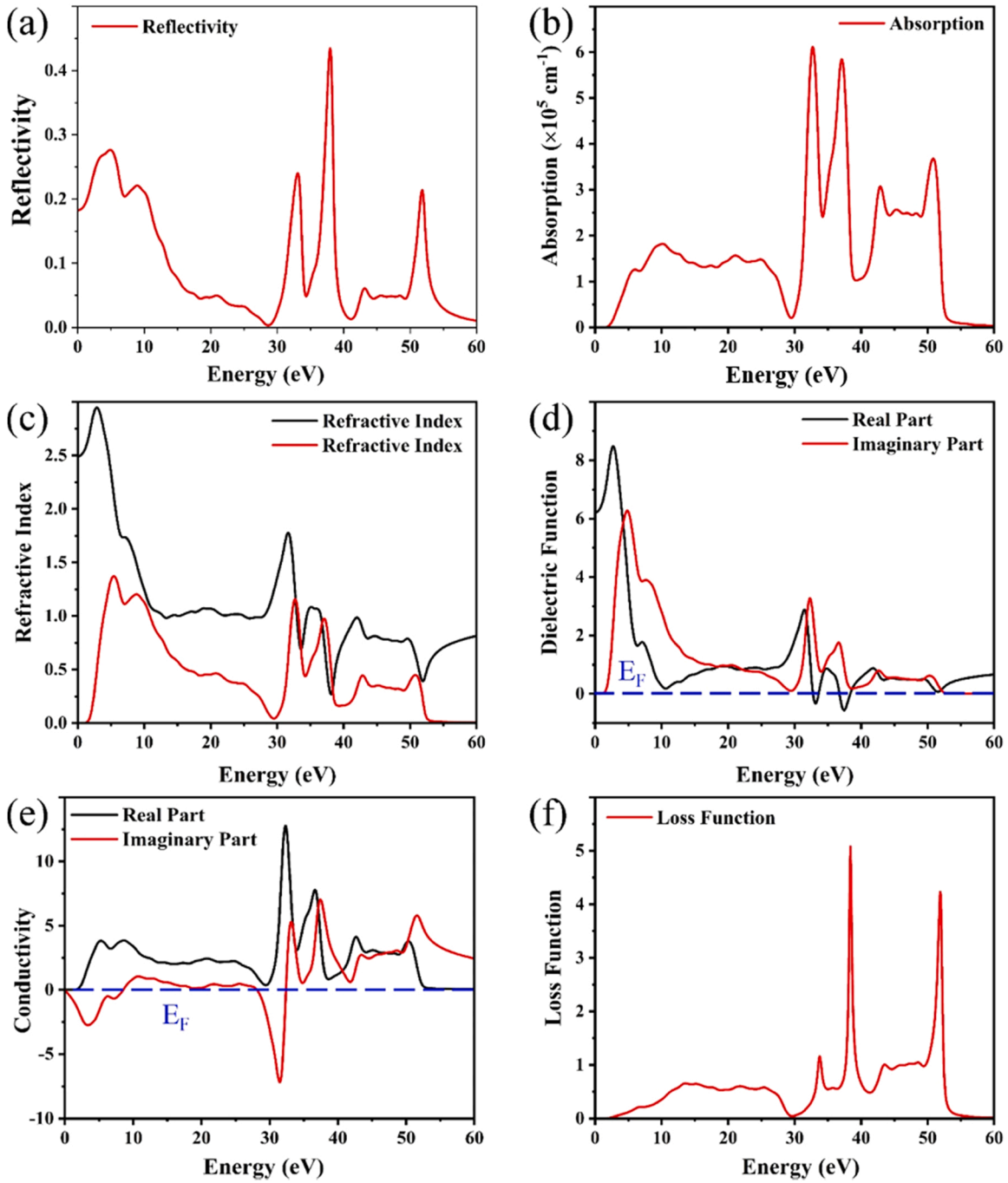

Fig. 4. Optical response of Hg_2WO_4 for the investigation of (a) reflectivity, (b) absorption, (c) refraction index, (d) dielectric function, (e) conductivity and (f) function of energy loss.

3.6. Refractive index

The expression used to calculate the refractive index n is given below:

$$n(\omega) = \left(\frac{1}{\sqrt{2}}\right)\left[\left\{\varepsilon_1{}^2 + \varepsilon_2{}^2/2\right\}^{\frac{1}{2}} + \varepsilon_1\right]^{\frac{1}{2}} \tag{5}$$

The complex refractive index consists of two parts: real and imaginary which can be expressed as:

$$N = n + ik \tag{6}$$

Here, n is refractive index and k is extinction coefficient. These parameters are frequency and hence energy dependent. Fig. 4(c) shows the dependence of real and imaginary parts of complex refractive index on energy. The refractive index and absorption are inversely related to each other. It is noticed that as the value of extinction coefficient k is increased, the absorption follows the same pattern and increases for the given range of energies, as shown in Fig. 4(b, c). The refractive index of Hg_2WO_4 is measured as 2.95 at 2.9 eV and 2.49 at 0 eV. The highest value of extinction coefficient k is found as 1.37 at 5.4 eV. Whereas, its value is recorded as 0 at 0 eV which shows that the process of annihilation of energy starts eventually as the light of suitable energy falls on the material.

3.7. Dielectric function

Dielectric function can be determined using the following relation:

$$\varepsilon(\omega) = \varepsilon_1(\omega) + i\varepsilon_2(\omega) \tag{7}$$

The value of dielectric function can directly be extracted from $\varepsilon_1(\omega)$ which can be obtained from Kramers-Kronig dispersion relation. The imaginary part $\varepsilon_2(\omega)$ can also be calculated from electronic band structure [53]. The behavior of real and imaginary parts of dielectric functions are shown in Fig. 4(d) which describe the polarization and dissipation of incident light. The value of $\varepsilon_2(\omega)$ is found as 0 at 0 eV and the major peak for $\varepsilon_2(\omega)$ with value 6.28 is observed at 4.8 eV. The real part of dielectric function has its value 6.19 at 0 eV while the highest peak of real part of complex dielectric function has a value as 8.48 at 2.72 eV.

3.8. Conductivity

Conductivity spectrum of Hg_2WO_4 is shown in Fig. 4(e). The relation used to determine conductivity of a material is shown in Eq. 7.

$$\sigma(\omega) = \frac{\omega}{4\pi}\varepsilon_2(\omega) \tag{8}$$

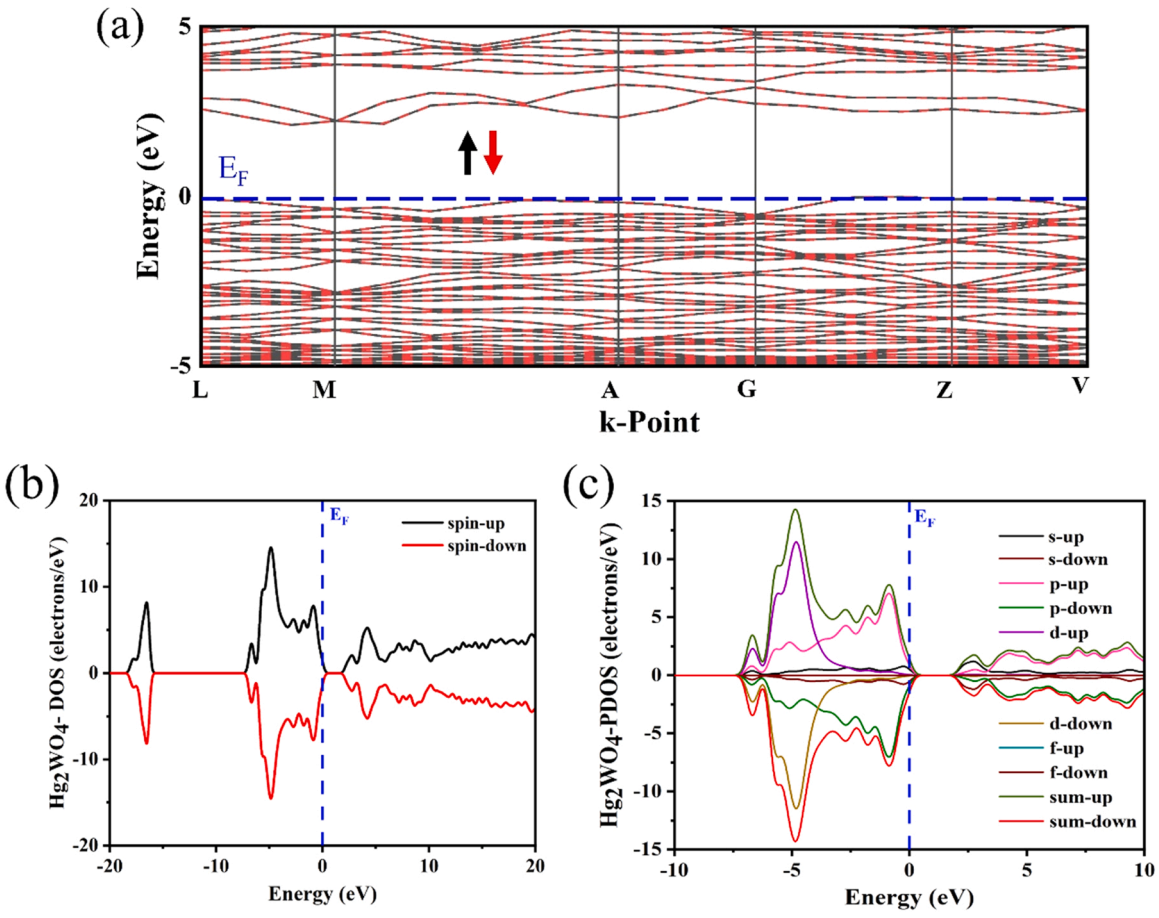

Fig. 5. Magnetic behavior of Hg_2WO_4: (a) spin-polarized energy band structure, (b) spin-polarized atomic DOS and (c) spin-polarized PDOS.

From calculation, it is noted that proposed material become highly conductive at 32.3 eV with conductivity 7.04. Also we can estimate resistivity of the given material just by reciprocating conductivity. The given material become highly resistive at 32.3 eV with resistivity of 0.14.

3.9. Loss function

When electron moves through the material, some of its energy is lost which is determined by function of energy loss denoted by L (ω). This function is also energy (frequency) dependent. The frequency associated to this loss function is termed as plasma frequency as it describes the characteristics of plasma resonance expression which relates the energy loss function and dielectric function as given below in Eq. 8 (54):

$$L(\omega) = \frac{\varepsilon_2(\omega)}{\varepsilon_1(\omega)^2 + \varepsilon_2(\omega)^2} \tag{9}$$

The spectrum for function of energy loss is given in Fig. 4(f) which shows the highest peak of loss function as 5.07 at 38.4 eV.

3.10. Magnetic properties

The magnetic features of Hg_2WO_4 are explored through application of magnetic field. GGA and PBE approach along with spin-polarized behavior is used for the calculations of Band Structure, DOS and PDOS of Hg_2WO_4. The magnetic behavior of an atom is determined through its spin and orbit coupled magnetic moments. The spin and orbital magnetic moments are associated with sinning of electrons about their own axes and orbital motion of electrons in Bohr's orbits. The combined effect of spin-orbit coupling contribute to magnetic characteristics of any material.

Fig. 5(a) shows the spin-polarized band gap curves of Hg_2WO_4 consisting of spin-up and spin-down energy states which determine the magnetic nature of a material. Formation of energy bands under the application of magnetic field are also shown in Fig. 5(b). The spin-up and spin-down states are mirror to each other. As the net magnetic dipole is zero, it can be suggested that the given material is antiferromagnetic in nature. Also, the net magnetization of this material is zero. The behavior of atomic orbitals of Hg_2WO_4 under the application of magnetic field is shown in Fig. 5(c). All the curves for spin-up and spin-down states of s, p, d, and f atomic orbitals are mirror to each other, and s-states have highest contribution while f-states have least contribution in magnetization of Hg_2WO_4.

4. Conclusions

The structural, elastic, electronic, optical and magnetic properties of perovskite-like Hg_2WO_4 are computationally studied. The structural properties show that the given compound has well stable structure and has a monoclinic arrangement of atoms. Ductile behavior of Hg_2WO_4 is confirmed with Pugh's approximation and Frantsevich's rule with values 2.02 and 0.28 respectively. The band gap of this material is found to be 2.14 eV which is indirect in nature. This outcome suggests that the given material has a good photosensitivity for visible light. The TDOS and elemental DOS of Hg_2WO_4 are identical. The Hg-5d is dominant in Hg-PDOS and O-2p is dominant in O-PDOS. Overall Hg-5d has a major contribution in PDOS with 22.7 states/eV. On spin-polarized treatment, Hg_2WO_4 shows antiferromagnetic behavior. The s-state has dominant contribution while f-state has least contribution in magnetization of Hg_2WO_4. The Hg_2WO_4 material gives notable response for absorption which evidences it as a potential candidate for photocatalytic hydrogen evolution reaction applications.

Declaration of Competing Interest

The authors declare the following financial interests/personal relationships which may be considered as potential competing interests: Adnan Khalil reports equipment, drugs, or supplies and writing assistance were provided by Khwaja Fareed University of Engineering & Information Technology.

Data availability

Data will be made available on request.

Acknowledgments

The authors extend their appreciation to the Deanship of Scientific Research at King Khalid University for funding this work through research groups program under grant number (RGP.1/378/42). In addition, the author (Soumaya Gouadria) Princess Nourah bint Abdulrahman University Researchers Supporting Project number (PNURSP2023R184), Princess Nourah bint Abdulrahman University, Riyadh, Saudi Arabia.

References

[1] L. Wang, J. Zhao, H. Liu, J. Huang, Design, modification and application of semiconductor photocatalysts, J. Taiwan Inst. Chem. Eng. 93 (2018) 590–602.

[2] Y. Huang, J. Liu, Y. Deng, Y. Qian, X. Jia, M. Ma, et al., The application of perovskite materials in solar water splitting, J. Semicond. 41 (1) (2020), 011701.
[3] D. Kwon, I. Yang, S. An, J. Cho, J.-M. Ha, J.C. Jung, A study on active sites of A2BO4 catalysts with perovskite-like structures in oxidative coupling of methane, Mol. Catal. 506 (2021), 111548.
[4] G. Nirala, D. Yadav, S. Upadhyay, Ruddlesden-Popper phase A2BO4 oxides: recent studies on structure, electrical, dielectric, and optical properties, J. Adv. Ceram. 9 (2) (2020) 129–148.
[5] X. Xu, Y. Pan, Y. Zhong, R. Ran, Z. Shao, Ruddlesden–Popper perovskites in electrocatalysis, Mater. Horiz. 7 (10) (2020) 2519–2565.
[6] J. Kim, J. Mun, C.M. Palomares García, B. Kim, R.S. Perry, Y. Jo, et al., Superconducting Sr2RuO4 thin films without out-of-phase boundaries by higher-order Ruddlesden–Popper intergrowth, Nano Lett. 21 (10) (2021) 4185–4192.
[7] S. Kahmann, E.K. Tekelenburg, H. Duim, M.E. Kamminga, M.A. Loi, Extrinsic nature of the broad photoluminescence in lead iodide-based Ruddlesden–Popper perovskites, Nat. Commun. 11 (1) (2020) 1–8.
[8] M. Sahu, S.K. Gupta, D. Jain, M. Saxena, R. Kadam, Solid state speciation of uranium and its local structure in Sr2CeO4 using photoluminescence spectroscopy, Spectrochim. Acta Part A Mol. Biomol. Spectrosc. 195 (2018) 113–119.
[9] S.-H. Pan, J.-J. Shi, M. Zhang, M. Wu, Y.-L. Cen, W.-H. Guo, et al., Photocatalytic performance enhancement of two-dimensional Ruddlesden-Popper type perovskite K2La2Ti3O10 by nitrogen-doping, Mater. Res. Express 6 (7) (2019), 075047.
[10] W. Wang, M. Xu, X. Xu, W. Zhou, Z. Shao, Perovskite oxide based electrodes for high-performance photoelectrochemical water splitting, Angew. Chem. Int. Ed. 59 (1) (2020) 136–152.
[11] H. Xiao, P. Liu, W. Wang, R. Ran, W. Zhou, Z. Shao, Enhancing the photocatalytic activity of Ruddlesden-Popper Sr2TiO4 for hydrogen evolution through synergistic silver doping and moderate reducing pretreatment, Mater. Today Energy 23 (2022), 100899.
[12] V. Dutta, S. Sharma, P. Raizada, V.K. Thakur, A.A.P. Khan, V. Saini, et al., An overview on WO3 based photocatalyst for environmental remediation, J. Environ. Chem. Eng. 9 (1) (2021), 105018.
[13] S. Chen, Y. Hu, S. Meng, X. Fu, Study on the separation mechanisms of photogenerated electrons and holes for composite photocatalysts g-C3N4-WO3, Appl. Catal. B Environ. 150 (2014) 564–573.
[14] J. Wen, N. Li, Q. Shi, H. Wu, X. Feng, C. Wang, et al., First-principles calculations to investigate electronic structures and magnetic regulation of non-metallic elements doped BP with point defects, J. Mol. Graph. Model. 118 (2023), 108370.
[15] W. Jeitschko, A.W. Sleight, The crystal structures of HgMoO4 and two forms of SnWO4, Z. Naturforsch. B 27 (2) (1972) 203.
[16] T.J. Mormann, W. Jeitschko, Mercury (I) molybdates and tungstates: Hg2WO4 and two modifications of Hg2MoO4, Inorg. Chem. 39 (19) (2000) 4219–4223.
[17] K. Radja, B.L. Farah, A. Ibrahim, D. Lamia, I. Fatima, B. Nabil, et al., Investigation of structural, magneto-electronic, elastic, mechanical and thermoelectric properties of novel lead-free halide double perovskite Cs2AgFeCl6: first-principles calcuations, J. Phys. Chem. Solids (2022), 110795.
[18] A. Khireddine, A. Bouhemadou, S. Maabed, S. Bin-Omran, R. Khenata, Y. Al-Douri, Elastic, electronic, optical and thermoelectric properties of the novel Zintl-phase Ba2ZnP2, Solid State Sci. 128 (2022), 106893.
[19] B. Asma, F. Belkharroubi, A. Ibrahim, B. Lamia, A. Mohammed, W. Belkilali, et al., Structural, mechanical, magnetic, electronic, and thermal investigations of Ag2YB (Y= Nd, Sm, Gd) full-Heusler alloys, Emerg. Mater. 4 (6) (2021) 1769–1783.
[20] A. Bekhti-Siad, K. Bettine, D.P. Rai, Y. Al-Douri, X. Wang, R. Khenata, et al., Electronic, optical and thermoelectric investigations of Zintl phase AE3AlAs3 (AE= Sr, Ba): first-principles calculations, Chin. J. Phys. 56 (3) (2018) 870–879.
[21] K. Boudiaf, A. Bouhemadou, Y. Al-Douri, R. Khenata, S. Bin-Omran, N. Guechi, Electronic and thermoelectric properties of the layered BaFAgCh (Ch= S, Se and Te): first-principles study, J. Alloy. Compd. 759 (2018) 32–43.
[22] A. Saim, F. Belkharroubi, F. Boufadi, I. Ameri, L. Blaha, A. Tebboune, et al., Investigation of the structural, elastic, electronic, and optical properties of half-Heusler CaMgZ (Z= C, Si, Ge, Sn, Pb) compounds, J. Electron. Mater. 51 (7) (2022) 4014–4028.
[23] L. Samia, F. Belkharroubi, A. Ibrahim, B.F. Lamia, A. Saim, A. Maizia, et al., Investigation of structural, elastic, electronic, and magnetic proprieties for X2LuSb (X= Mn and Ir) full-Heusler alloys, Emerg. Mater. 5 (2) (2022) 537–551.
[24] Y. Al-Douri, M. Ameri, A. Bouhemadou, K.M. Batoo, First-principles calculations to investigate the refractive index and optical dielectric constant of Na3SbX4 (X= S, Se) ternary chalcogenides, Phys. Status Solidi (b) 256 (11) (2019) 1900131.
[25] A. Khireddine, A. Bouhemadou, S. Alnujaim, N. Guechi, S. Bin-Omran, Y. Al-Douri, et al., First-principles predictions of the structural, electronic, optical and elastic properties of the zintl-phases AE3GaAs3 (AE= Sr, Ba), Solid State Sci. 114 (2021), 106563.
[26] M. Ameri, F. Bennar, S. Amel, I. Ameri, Y. Al-Douri, D. Varshney, Structural, elastic, thermodynamic and electronic properties of LuX (X= N, Bi and Sb) compounds: first principles calculations, Phase Transit. 89 (12) (2016) 1236–1252.
[27] B. Fadila, M. Ameri, D. Bensaid, M. Noureddine, I. Ameri, S. Mesbah, et al., Structural, magnetic, electronic and mechanical properties of full-Heusler alloys Co2YAl (Y= Fe, Ti): first principles calculations with different exchange-correlation potentials, J. Magn. Magn. Mater. 448 (2018) 208–220.
[28] A. Fakharuddin, U. Shabbir, W. Qiu, T. Iqbal, M. Sultan, P. Heremans, et al., Inorganic and layered perovskites for optoelectronic devices, Adv. Mater. 31 (47) (2019) 1807095.
[29] A.E. Fedorovskiy, N.A. Drigo, M.K. Nazeeruddin, The role of Goldschmidt's tolerance factor in the formation of A2BX6 double halide perovskites and its optimal range, Small Methods 4 (5) (2020) 1900426.
[30] M. Liang, W. Lin, Z. Lan, J. Meng, Q. Zhao, X. Zou, et al., Electronic structure and trap states of two-dimensional ruddlesden–popper perovskites with the relaxed Goldschmidt tolerance factor, ACS Appl. Electron. Mater. 2 (5) (2020) 1402–1412.
[31] T.J. Huang, Z.X. Thiang, X. Yin, C. Tang, G. Qi, H. Gong, (CH3NH3) 2PdCl4: a compound with two-dimensional organic–inorganic layered perovskite structure, Chem. Eur. J. 22 (6) (2016) 2146–2152.
[32] Kumar U. Synthesis and Characterization of Undoped and Doped Layered Perovskite Oxides Sr2SnO4: IIT BHU; 2019.
[33] L. Hasni, M. Ameri, D. Bensaid, I. Ameri, S. Mesbah, Y. Al-Douri, et al., First-principles calculations of structural, magnetic electronic and optical properties of rare-earth metals TbX (X= N, O, S, Se), J. Supercond. Nov. Magn. 30 (12) (2017) 3471–3479.
[34] M. Benkabou, M. Harmel, A. Haddou, A. Yakoubi, N. Baki, R. Ahmed, et al., Structural, electronic, optical and thermodynamic investigations of NaXF3 (X= Ca and Sr): first-principles calculations, Chin. J. Phys. 56 (1) (2018) 131–144.
[35] I. Yahiaoui, A. Lazreg, Z. Dridi, Y. Al-Douri, B. Bouhafs, Gd impurities effect on $$\hbox {Co} _ {2}\hbox {CrSi} $$ Co 2 CrSi alloy: first-principle calculations, Bull. Mater. Sci. 41 (1) (2018) 1–5.
[36] Y. Benkaddour, A. Abdelaoui, A. Yakoubi, H. Khachai, Y. Al-Douri, S.B. Omran, et al., First-principle calculations of structural, elastic, and electronic properties of intermetallic rare earth R2Ni2Pb (R= Ho, Lu, and Sm) compounds, J. Supercond. Nov. Magn. 31 (2) (2018) 395–403.
[37] M.J. Rutter, C2x: a tool for visualisation and input preparation for Castep and other electronic structure codes, Comput. Phys. Commun. 225 (2018) 174–179.
[38] K. Boudiaf, A. Bouhemadou, O. Boudrifa, K. Haddadi, F.S. Saoud, R. Khenata, et al., Structural, elastic, electronic and optical properties of LaOAgS-type silver fluoride chalcogenides: first-principles study, J. Electron. Mater. 46 (7) (2017) 4539–4556.
[39] Z. Souadia, A. Bouhemadou, R. Khenata, Y. Al-Douri, Structural, elastic and lattice dynamical properties of the alkali metal tellurides: first-principles study, Phys. B Condens. Matter 521 (2017) 204–214.
[40] K. Bidai, M. Ameri, S. Amel, I. Ameri, Y. Al-Douri, D. Varshney, et al., First-principles calculations of pressure and temperature dependence of thermodynamic properties of anti-perovskite BiNBa3 compound, Chin. J. Phys. 55 (5) (2017) 2144–2155.
[41] Woods N., Payne M., Hasnip P., editors. The Self-Consistent Field in Kohn-Sham Density Functional Theory: A Review of Methods and Algorithms. APS March Meeting Abstracts; 2019.
[42] S.L. Wang, Y. Pan, Insight into the structures, melting points, and mechanical properties of NbSi2 from first-principles calculations, J. Am. Ceram. Soc. 102 (8) (2019) 4822–4834.
[43] M.C. Payne, M.P. Teter, D.C. Allan, T. Arias, A.J. Joannopoulos, Iterative minimization techniques for ab initio total-energy calculations: molecular dynamics and conjugate gradients, Rev. Mod. Phys. 64 (4) (1992) 1045.

[44] S. Shafiq, A. Hussain, M.N. Rasul, S.S. Hayat, F. Iqbal, M.A. Rafiq, First-principles structural, electronic, optical and bonding properties of scandium-based ternary indide system Sc5T2In4 (T= Ni, Pd, Pt), Bull. Mater. Sci. 43 (1) (2020) 1–10.
[45] M. Ayad, F. Belkharroubi, F. Boufadi, M. Khorsi, M. Zoubir, M. Ameri, et al., First-principles calculations to investigate magnetic and thermodynamic properties of new multifunctional full-Heusler alloy Co2TaGa, Indian J. Phys. 94 (6) (2020) 767–777.
[46] A. Moussali, M.B. Amina, B. Fassi, I. Ameri, M. Ameri, Y. Al-Douri, First-principles calculations to investigate structural and thermodynamic properties of Ni2LaZ (Z= As, Sb and Bi) Heusler alloys, Indian J. Phys. 94 (11) (2020) 1733–1747.
[47] N. Guechi, A. Bouhemadou, Y. Medkour, Y. Al-Douri, R. Khenata, S. Bin-Omran, Electronic and thermoelectric properties of the layered Zintl phase CaIn2P2: first-principles calculations, Philos. Mag. 100 (23) (2020) 3023–3039.
[48] A. Mentefa, F.Z. Boufadi, M. Ameri, F. Gaid, L. Bellagoun, A.A. Odeh, et al., First-principles calculations to investigate structural, electronic, elastic, magnetic, and thermodynamic properties of full-heusler Rh2MnZ (Z= Zr, Hf), J. Supercond. Nov. Magn. 34 (1) (2021) 269–283.
[49] M. Rizwan, I. Zeba, M. Shakil, S. Gillani, Z. Usman, Electronic, structural and optical properties of BaTiO3 doped with lanthanum (La): insight from DFT calculation, Optik 211 (2020), 164611.
[50] W. Belkilali, F. Belkharroubi, M. Ameri, N. Ramdani, F. Boudahri, F. Khelfaoui, et al., Theoretical investigations of structural, mechanical, electronic and optical properties of NaScSi alloy, Emerg. Mater. 4 (5) (2021) 1465–1477.
[51] S.A. Dar, V. Srivastava, U.K. Sakalle, Structural, elastic, mechanical, electronic, magnetic, thermoelectric and thermodynamic investigation of half metallic double perovskite oxide Sr2MnTaO6, J. Magn. Magn. Mater. 484 (2019) 298–306.
[52] M.H. Rubel, M.M. Ali, M. Ali, R. Parvin, M. Rahaman, K. Hossain, et al., First− principles study: structural, mechanical, electronic and thermodynamic properties of simple− cubic− perovskite (Ba0. 62K0. 38)(Bi0. 92Mg0. 08) O3, Solid State Commun. 288 (2019) 22–27.
[53] M. Rizwan, Z. Usman, M. Shakil, S. Gillani, S. Azeem, H. Jin, et al., Electronic and optical behaviour of lanthanum doped CaTiO3 perovskite, Mater. Res. Express 7 (1) (2020), 015920.
[54] J.U. Rehman, M. Usman, M.B. Tahir, A. Hussain, M.A. Rehman, M. Sagir, et al., First-principles calculations to investigate ultra-wide bandgap semiconductor behavior of NaMgF3 fluoro-perovskite with external static isotropic pressure and its impact on optical properties, Optik 252 (2022), 168532.